An Sn-induced resonant level in β-As2Te3

Bartlomiej Wiendlocha, Jean-Baptiste Vaney, Christophe Candolfi, Anne Dauscher, Bertrand Lenoir, Janusz Tobola

Sn-induced resonant level in β-As_2Te_3

Bartlomiej Wiendlocha[1,a], Jean-Baptiste Vaney[2], Christophe Candolfi[2], Anne Dauscher[2], Bertrand Lenoir[2] , Janusz Tobola[1]

[1] *Faculty of Physics and Applied Computer Science, AGH University of Science and Technology, Al. Mickiewicza 30, 30-059 Krakow, Poland*

[2] *Institut Jean Lamour, UMR 7198 CNRS – Université de Lorraine, 2 allée André Guinier – Campus ARTEM, 54000 Nancy, France*

[(a)] Corresponding author: wiendlocha@fis.agh.edu.pl

Abstract

Distortion of the density of states by an impurity-induced resonant level has been shown to provide an effective strategy to improve the thermoelectric performance of semiconductors such as Bi_2Te_3, PbTe or SnTe. Here, combining first-principles calculations and transport properties measurements, we demonstrate that Sn is a resonant impurity that distorts the valence band edge in *p*-type β-As_2Te_3. This remarkable effect is characterized as a prominent, sharp peak in the electronic density of states near the Fermi level. To illustrate the particular influence of Sn on the thermopower of β-As_2Te_3, the theoretical Ioffe-Pisarenko curve, computed within the Boltzmann transport theory, is compared with experimental results obtained on three series of polycrystalline samples with substitution of Ga and Bi for As and I for Te. While Ga and I behave as conventional, rigid-band-like dopants and follow the theoretical predictions, Sn results in significant deviations from the theoretical curve with a clear enhancement of the thermopower. Both electronic band structure calculations and transport properties measurements provide conclusive evidence that this enhancement and hence, the good thermoelectric performances achieved at mid temperatures in β-$As_{2-x}Sn_xTe_3$ can be attributed to resonant level induced by Sn atoms.

The possibility to induce resonant states in the electronic band structure of β-As_2Te_3 opens new avenues to further optimize its thermoelectric performances.

1. Introduction

The conversion of different forms of energy using crystalline materials is a fascinating subject that still focuses significant theoretical and experimental efforts. Such effects usually involve complex phenomena in condensed matter physics typified by a subtle interplay between structural, electrical, magnetic and thermodynamic degrees of freedom. Among such materials, thermoelectric (TE) alloys are extremely attractive systems, as they allow direct conversion of heat into electricity and *vice versa*. The efficiency of a TE system is conveniently expressed by the dimensionless thermoelectric figure of merit $ZT = S^2T/\rho\kappa$, where S, ρ, κ and T are the Seebeck coefficient (or thermopower), the electrical resistivity, the total thermal conductivity and the absolute temperature, respectively. All these physical quantities strongly vary with the electron (*n*-type) or hole (*p*-type) concentration and temperature. For this reason, first-principles calculations of the electronic and thermal properties of TE materials are particularly desirable, since they enlighten the key mechanisms governing their TE properties and provide guidance to further optimize them.

The use of certain unique features of the electronic band structure in the vicinity of the Fermi level (E_F) is a well-established strategy to enhance the power factor S^2/ρ through band convergence, band alignment or the formation of resonant levels (RL), all of which can be manipulated by introducing judicious dopants. RL are formed by certain impurity atoms in a semiconductor which modify the electronic structure of the host material beyond the rigid-band model[1]. The manifestation of the formation of RL is a sharp and narrow peak in the electronic density of states (DOS) at the resonance energy, when the impurity concentration is very low (*e.g.* 0.1 %). When the impurity concentration that induce RL is further increased, the narrow DOS peak hybridizes with the electronic

states of the host crystal, forming a broader maximum in the DOS curve, which may lead to an increase in the thermopower for a given carrier concentration. The well-known examples of thermoelectric materials with resonant impurities are Sn-doped Bi_2Te_3[2], Tl-doped PbTe[3,4], or In-doped SnTe[5], where a significant increase in thermopower due to resonant level were reported, leading to enhanced *ZT* values in the two latter cases (*ZT* was not measured in Sn-doped Bi_2Te_3). An important issue, however, regarding resonant impurities, is how to select properly such impurity to obtain good transport properties. Such a "proper selection" of the resonant state should be primarily understood as the tendency of RL towards hybridization with the host electronic states, in order to avoid localization effects, as observed, for instance, with 3*d* transition metal impurities in IV-VI semiconductor (like titanium in PbTe, shown[6,7,8] to be such a "bad RL" example). A "rule of thumb" for a proper selection is a similar orbital momentum character of the impurity and host electronic states, that is, RL should be formed by *s*- or *p*-like states in *sp* semiconductors, such as PbTe or Bi_2Te_3. In such a case, the increase in thermopower may be qualitatively explained in several equivalent ways. Firstly, the distortion and increase in DOS enhances the DOS effective mass m^* and lowers E_F values for a given charge carrier concentration, leading to an increase in the thermopower that roughly scales as[3,4] $\sim m^*$ and $\sim 1/E_F$. Secondly, the formation of such a DOS distortion may increase the energy derivative $dn/dE \sim S$, where *n* is the number of electronic states near E_F[1,3]. Finally, the properly selected RL does not form an isolated impurity band, but increases the number of electronic states available for charge transport near the original valence (conduction) band, and hence, may increase the thermopower in a similar way as band convergence.[8,9,] The hybridization and similar angular momentum number of the impurity and host states also help to avoid enhanced scattering on the RL, which would reduce the mobility of the charge carriers. In practice, scattering on RL, very strong at low temperatures, becomes comparable to the electron-phonon scattering at room and elevated temperatures, as discussed for PbTe:Tl for instance.[10] The experimental verification for such a positive resonant effect is notably obtained via an increase in thermopower at a given carrier concentration in the system doped with RL compared to

other, non-resonant (rigid-band-like) impurities. This effect can be conveniently visualized on a Ioffe-Pisarenko plot where a departure from the conventional carrier concentration dependence of the thermopower is observed.

As Bi_2Te_3, the binary As_2Te_3 belongs to the tetradymite family of compounds which are still to date the best materials for room- and mid-temperature thermoelectric applications.[11] Under ambient pressure, As_2Te_3 is polymorphic and crystallizes with two possible structures denoted as the α phase, which is monoclinic (space group $C2/m$), and the β phase, which adopts a rhombohedral crystal structure (space group $R\bar{3}m$, see Figure 1) similar to Bi_2Te_3. Low-temperature X-ray and neutron diffraction have further revealed that the β phase undergoes a displacive transformation upon cooling below 200 K to a structure described in the monoclinic space group $P2_1/m$ (phase referred to as β'). Recent investigations [12,13,14,15,16,17,18] on the thermoelectric properties of both structure types evidenced semiconducting-like electronic properties and very low lattice thermal conductivity on the order of 0.7 and 0.5 W m^{-1} K^{-1} at 300 K for the α and β phase, respectively. Thanks to this favorable combination of transport properties and the possibility to adjust the hole concentration through substitution of Sn for As, good thermoelectric performances with maximum *ZT* values of 0.80 at 523 K and 0.65 at 423 K were achieved in the α and β phase, respectively. These studies have also highlighted the important influence of defects (vacancies and/or antisite defects) on the transport properties of both compounds. The strong similarities in the crystal structure and defect chemistry between β-As_2Te_3 and Bi_2Te_3 naturally raise the question of whether Sn induces RL in β-As_2Te_3 as it does in Bi_2Te_3.

Here, we provide both theoretical and experimental evidences that Sn indeed acts similarly and give rise to RL in the valence bands of β-As_2Te_3. Our electronic structure calculations show, that Sn forms a resonant peak in the density of states of β-As_2Te_3. To illustrate the distinct role of Sn on the thermopower, the transport properties measurements reported for the series β-$As_{2-x}Sn_xTe_3$ (x = 0.0, 0.015, 0.025, 0.035 and 0.050) are contrasted with those determined on gallium (β-$As_{2-y}Ga_yTe_3$; y =

0.01 and 0.03), bismuth (β-$As_{2-n}Bi_nTe_3$; n = 0.015 and 0.025) and iodine (β-$As_2Te_{3-z}I_z$; z = 0.01 and 0.02) substituted samples. Theoretical calculations of the electronic structure and transport properties of pristine β-As_2Te_3 were additionally performed. The results show that the Ioffe-Pisarenko plot predicted by calculations backs up the experimental results for the Ga-, Bi- and I-containing samples but underestimates the thermopower of Sn-doped samples. This enhancement of thermopower evidences that the Sn-induced distortion of the density of states enables achieving higher S values than obtained for conventional, rigid-band-like impurities.

2. Experimental and computational details

First-principles calculations were done with the help of two complementary methods, KKR-CPA and FP-LAPW. By using the Korringa-Kohn-Rostoker (KKR) method with the coherent potential approximation [19, 20] (CPA) to treat explicitly the chemical disorder on the As sublattice, which accompanies the substitution of Sn for As, resonant level was identified, and its evolution with varying Sn content was studied. The exchange-correlation potential was computed using the Perdew-Wang formula[21] in the local density approximation (LDA). Within the KKR-CPA formalism, the electronic structure calculations for the doped material are done in a primitive cell of the pristine compound by using the effective Green's function technique, and the computed properties are automatically averaged over all possible configurations[19]. The fully charge self-consistent crystal potentials were constructed in the muffin-tin form. The position of the Fermi level was determined accurately by the generalized Lloyd formula[22].

To study the relaxation effects around the impurity, as well as to compute the transport properties of pristine β-As_2Te_3, the full-potential linearized-augmented plane wave method (FP-LAPW) implemented in the WIEN2k package[23] was used. The modified Becke–Johnson semilocal exchange potential of Tran and Blaha[24] was applied. Transport properties were computed using the

Boltzmann approach with the BoltzTraP[25] code. The crystal structure of pristine β-As_2Te_3 was relaxed before computations. The computed structural parameters are gathered in Table I.

Polycrystalline samples of β-$As_{2-y}Ga_yTe_3$ and β-$As_2Te_{3-z}I_z$ were synthesized similarly to the β-$As_{2-x}Sn_xTe_3$ and β-$As_{2-n}Bi_nTe_3$ series.[12,17,26] First, the mixtures of high-purity powders of the elements were weighed in appropriate stoichiometric ratios and heated in sealed evacuated quartz tubes at a rate of 10 K min^{-1} to 923 K in a rocking furnace. The tubes were held at this final temperature for 2 h and quenched in icy water. The as-prepared ingots were reground into micron-sized powders and cold-pressed into cylindrical pellets of 10 mm in diameter under a pressure of 750 MPa. Regardless of the nature of the substituting element, the obtained cylinders showed an experimental density higher than 92% of the theoretical density determined from crystallographic data.

The nature and phase purity of the samples were determined by powder X-ray diffraction (PXRD) using a Bruker D8 Advance instrument (CuKα_1 radiation). The chemical homogeneity of the samples was assessed by scanning electron microscopy (SEM) and energy dispersive X-ray (EDX) mapping using a Quanta FEG 650 (FEI).

For transport properties measurements, the dense cylinders were cut both parallel and perpendicular to the pressing direction into bar-shaped samples of dimensions 2×2×8 mm^3 due to the anisotropic crystal structure of β-As_2Te_3. Measurements of the thermopower were performed at 300 K in a physical property measurement system (PPMS, Quantum Design) with the thermal transport option (TTO). To this end, four copper leads were attached onto the samples with a low-melting-point braze. The hole carrier concentrations were measured using the ac transport option of the PPMS by a five-probe method. Five copper wires were glued onto the samples with a low-melting-point braze. The Hall resistivity ρ_H was determined from measurements of the transverse electrical resistivity ρ_{xy} under magnetic fields $\mu_0 H$ ranging between +1 and -1T. The data were subsequently corrected to dismiss magnetoresistive contributions due to misalignments of the contacts following the formula $\rho_H =$

$[\rho_{xy}(\mu_0 H) - \rho_{xy}(-\mu_0 H)]/2$. The Hall coefficient R_H was determined from the slope of the $\rho_H(\mu_0 H)$ data in the limit $\mu_0 H \to 0$. The Hall carrier concentration p was then inferred within a single-band approximation by the formula $p = 1/R_H e$, where e is the elementary charge. The experimental uncertainty in the thermopower and Hall effect measurements is estimated to be 5%. As shown in prior studies, the anisotropy in the thermopower and in the Hall coefficient is very low and at the border of the experimental uncertainty of these measurements. Our theoretical transport calculations discussed in the following section will further support this statement. Hereafter, only the values measured in the parallel direction will be shown for clarity, keeping in mind that the conclusions drawn are not affected if the values measured perpendicular to the pressing direction were to be considered.

The structural and chemical characterizations performed on samples of the Sn and Bi series can be found in Refs. [12, 17, 26]. A detailed presentation and discussion of the results obtained on the series β-$As_{2-y}Ga_yTe_3$ and β-$As_2Te_{3-z}I_z$ will be the subject of a forthcoming paper. We therefore only report herein the properties relevant for the present discussion and the demonstration of the appearance of RL induced by Sn in β-As_2Te_3. The PXRD, SEM and EDX analyses carried out on the samples of the Ga and I series confirmed the successful synthesis of the targeted compositions and indicated a good chemical homogeneity evidenced by a homogeneous spatial distribution of the elements within the As_2Te_3 matrix. Only small fractions of AsTe (less than 1% in volume) was visible in the PXRD patterns for some compositions. The distribution of iodine could not be probed by EDX due to the low doping levels and strong peak overlapping between I and Te. However, its insertion into the crystal structure of β-As_2Te_3 was confirmed by an increase in the unit cell volume determined by Rietveld refinements of the PXRD data. These results provide experimental evidence that Ga and I substitute for As and Te, respectively, in β-As_2Te_3 and ensure that the thermopower measured as well as its variations with the substitution level are intrinsic to the β phase of As_2Te_3.

3. Results and discussion

3.1 Electronic band structure

Figure 2 shows the computed electronic density of states for β-$As_{1.999}Sn_{0.001}Te_3$ (panels a-c) and β-$As_{1.98}Sn_{0.02}Te_3$ (panel d). The electronic band structure of pristine β-As_2Te_3 is in general agreement with that reported in previous studies[18,27], and is discussed in next paragraphs. For a Sn doping level of x = 0.001, a sharp resonance peak is clearly seen (panels a-c). Hybridization effects occur when the doping level is increased to x = 0.02, which corresponds to substitution levels studied experimentally[12]. This resonant state is formed by 5*s* orbitals of Sn (Figure 2b) in analogy to the RL observed in Sn-doped Bi_2Te_3 [28]. In the lower energy range, a second, hyper-deep resonant state (HDS) is formed near -7.5 eV (Figure 2c), which is characteristic in such systems [28]. Thanks to the formation of this hyper-deep state, Sn, which has four valence electrons (two on 5*s* and two on 5*p* orbitals), becomes a monovalent acceptor against trivalent As in As_2Te_3. HDS bounds one electron from Sn and one electron from As, thus effectively only two electrons are delivered to the valence band per each Sn atom. As a result, Sn acts as Sn^{2+}, in a way similar to that observed in Sn-doped Bi [29]. An important feature regarding the transport properties of this system is the relatively broad DOS maximum which is formed when the impurity concentration is increased to x = 0.02 (Figure 2d). This broad maximum replaces the narrow DOS peak observed for x = 0.001 in Figure 2a. The strong hybridization of the resonant peak with the electronic states of the host material manifests itself in the partial component densities of states computed for x = 0.02. At the Fermi level E_F, the relative contribution to the total DOS from each kind of atoms amounts to about 6% for Sn, 15% for As, and 53% for Te (these values correspond to the ratio of the partial DOS, weighted by atomic concentration, to the total DOS; the remaining part is distributed in the interstitial region). Thus, similarly to Tl-doped PbTe1,4,9, the resonant impurity only "catalyzes" the formation of the DOS hump, with a small contribution from its

own electronic states, thereby increasing the number of mobile charge carriers available for the electrical and heat conductions. This allows to avoid any localization issues and provides a possibility to improve thermoelectric transport properties.

While our KKR-CPA computations predict the formation of RL by Sn in β-As_2Te_3, the crystal lattice relaxation effects are not taken into account within the coherent potential approximation. Hence, as a consistency check, we performed additional calculations to determine the influence of crystal lattice relaxation around Sn atoms in the β-As_2Te_3 matrix on the formation of the resonant state. To this end, we performed FP-LAPW calculations on a 135-atom hexagonal supercell with a single As atom replaced by Sn. The supercell was constructed by multiplying the hexagonal unit cell of the initially optimized As_2Te_3 by 3×3×1 (see Table I for the crystallographic parameters used), and by substituting one Sn atom for As. The symmetry was reduced due to the Sn/As substitution, and the final supercell belonged to the space group $P3m1$ (no. 156). Atomic positions in the supercell were next relaxed until the force, acting on each atom, was smaller than 10^{-3} Ry a_B^{-1} (where a_B is Bohr radius). Since the atomic radius of Sn is slightly larger than that of As (140 pm compared to 119 pm), a small increase in the distance between Sn and its nearest (NN) and next-nearest neighbors (NNN; Te atoms in both cases) was found: from 2.85 to 3.00 Å and 3.00 to 3.08 Å, respectively. The effect of further neighboring atoms was negligible. For the relaxed supercell, computations were performed taking into account the spin-orbit coupling (SOC). The calculated density of states, shown in Figure 3, clearly indicate that RL is robust against crystal structure relaxation, and not affected by the SOC. The lack of influence of SOC is consistent with the fact that RL is related to *s*-like orbitals of Sn, which are not directly involved in the spin-orbit interaction. We note that subtle differences between the DOS computed by the KKR-CPA and FP-LAPW methods exist when comparing Figures 2 and 3. They are related to differences in exchange-correlation potentials, shape of potential and the use of supercell geometry in FP-LAPW. Nevertheless, both theoretical methods consistently predict the formation of

resonant states from the 5*s* states of Sn atoms in β-As_2Te_3.

In order to analyze in more details the experimental data described below, the Fermi surface and thermopower of pristine β-As_2Te_3 were additionally computed. Figure 4 presents the electronic band structure near the band gap, and Figure 5 shows *p*- and *n*-type Fermi surfaces (FS) for selected carrier concentrations. Compared to sister tetradymite compounds, FS of *p*-type β-As_2Te_3 is very similar to Bi_2Te_3, with 6 ellipsoidal FS pockets for the lowest carrier concentrations, which evolve into more complex shapes with increasing *p*. The calculated band gap is indirect, and equal to E_g = 0.3 eV in agreement with prior studies [18,26]. The valence band maximum (VBM) is located on the so-called "mirror plane" close to the Z-F line and the top of the Brillouin zone, similarly to what was found[11] in Bi_2Te_3 and Sb_2Te_3. The conduction band minimum (CBM) is also on the mirror plane, at a *k*-point very close to, but not identical to that for the valence band, making the gap only "slightly" indirect. This is visualized in Fig. 5d, where small isoenergetical surfaces for the valence and conduction band at 2 meV below (above) the band edge are plotted. As observed in this figure, the two surfaces do not overlap. The second maximum of the CB, very close in energy to the first one, is located at the Γ point, and gives rise to additional FS ellipsoidal pocket, appearing at higher electron concentrations in the center of the Brillouin zone, as shown in Fig. 5(e).

A comparison of our computed band gap with that determined in some of the prior theoretical studies indicate differences. In Ref. [27], a direct band gap of 0.22 eV was found, while in Ref. [30], a significantly lower value was obtained (E_g = 0.12 eV). The differences between our and previous results come from the differences in relaxed crystal structures, as well as different exchange-correlation potentials used. This evidences that positions of the band maxima in this system are very sensitive to the computational details, similar to what was found in other related tetradymites[11], *i.e.* Bi_2Te_3, Bi_2Se_3 and Sb_2Te_3. Unfortunately, no experimental measurements of the band gap has been reported so far for β-As_2Te_3 (Ref. [27] erroneously cites 0.13 eV as the experimental value of the band gap in β-As_2Te_3

while the reference quoted [30] does not confirm this).

Figure 6 presents the energy-dependent conductivity (the so-called transport function, TF) divided by the scattering time, $\sigma(E)/\tau$, computed with BoltzTraP[25], along the binary (a) and trigonal (c) axes. This TF is used below to compute other transport properties of the system, namely the thermopower and the Hall resistivity. Although TF is anisotropic, the anisotropy is not strong with generally $\sigma_a(E) > \sigma_c(E)$. This fact is related to the shape of the Fermi surfaces which are slightly elongated along the trigonal axis (Γ-Z direction), especially for *n*-type. In Figure 7, the room-temperature Hall carrier concentration $n_H = 1/eR_H$ is plotted for both *n*- and *p*-type β-As_2Te_3, along the two principal directions. Computations of the Hall coefficient R_H takes into account the actual Fermi surface geometry, but neglects carrier scattering effects. In the 10^{18} cm^{-3} – 10^{20} cm^{-3} concentration range, deviations from the *x* = *y* line (*i.e.* nominal = Hall carrier concentration), are very small confirming the very weak anisotropy in R_H. This ensures that the experimental Hall carrier concentrations, determined for the parallel direction as discussed in the Experimental section, can be considered as the actual concentration of holes in the samples studied.

The thermopower, computed using the constant scattering time approximation (CSTA), is plotted in Fig. 8 (a). As observed experimentally (see below), the anisotropy in the thermopower is negligible and becomes only significant for either low or high carrier concentrations. For lower carrier concentrations, it is important only at elevated temperatures, when the bipolar conductivity turns on. To take a look at the thermoelectric potential of β-As_2Te_3, the average power factor (PF) over the scattering time ($PF/\tau = S^2\sigma/\tau$) is plotted in Fig. 8 (b), and compared to Bi_2Te_3 (for the details of computations for Bi_2Te_3 see Ref. [11]). PF is averaged according to a "parallel" random grains model[32], $PF = \frac{\sigma_x S_x^2 + \sigma_y S_y^2 + \sigma_z S_z^2}{3}$. For *p*-type compounds, the PF of β-As_2Te_3 is slightly lower than in Bi_2Te_3, but this effect may be compensated in *ZT* by the thermal conductivity, which is lower in β-As_2Te_3. Interestingly, *n*-type compounds are predicted to have larger PF values than Bi_2Te_3, suggesting that

potentially good TE performances may be achieved, especially if heavily-doped samples can be synthesized.

Figure 9 presents the evolution of the density-of-states effective mass m^*_{DOS}, computed using the formula[31,32] $m_e m^*_{DOS} = \hbar^3 \pi^2 \sqrt[3]{g(E)g'(E)}$ where m_e is the free electron mass, $\hbar$ is the reduced Planck constant, $g(E)$ is the density of states per energy and volume and $g'(E)$ is its energy derivative. Between p = 10^{19} and 10^{20} cm^{-3}, m^*_{DOS} varies in the range 1.0 – 1.5 m_e, similarly to *p*-type Bi_2Te_3 (plotted in Fig. 9 after Ref. [11]).

3.2 Ioffe-Pisarenko plot

The room-temperature thermopower measured on the series β-$As_{2-x}Sn_xTe_3$ is shown in Figure 10. For comparison, the results obtained on the two present series (Ga and I) and those previously reported on the solid solution β-$As_{2-x}Bi_xTe_3$ (Refs. 17 and 26) have been added. The exact values of the dopant concentrations, carrier concentrations and thermopowers, are presented in Table 2. While I is expected to behave as an electron donor, both Ga and Bi (isoelectronic with As) are believed to change the amount of native *p*-type defects in β-As_2Te_3, the nature of which is probably As_{Te} antisite defects in the Te outer, weakly-bounded "van der Waals" atomic layer[33]. These experimental values are further compared with two theoretical Ioffe-Pisarenko curves, which were generated for pristine β-As_2Te_3. The first curve is a conductivity-weighted average thermopower from Fig. 8(a) within the constant scattering time approximation (CSTA), while the second curve has been calculated using a single parabolic band (SPB) model assuming acoustic phonon scattering and a constant density-of-states effective mass m^*_{DOS} of 1.14m_e which corresponds well with the m^*_{DOS} computed in Fig. 9. As evidenced in Figure 10, the same m^*_{DOS} value describes quite well the measured thermopower values of the Ga-, Bi- and I-substituted samples. The fact that a single m^*_{DOS} value describes adequately the variations in the thermopower with p is consistent with our calculations indicating a nearly parabolic

valence band dispersion in this hole concentration range. In spite of a slight overestimation of the thermopower, the CSTA agrees also well with the experimental data for the three series with Ga, I and Bi. The small discrepancy observed between theory and experiment is not surprising, since acoustic phonon scattering that dominates in β-As_2Te_3 is not taken into account in our Boltzmann calculations. In this case, the CSTA is expected to overestimate the thermopower values, as it was observed in Bi_2Te_3 in Ref [11]. However, the experimental results obtained on the Sn-substituted samples are in stark contrast with theoretical predictions. The experimental values are larger than the computed ones across the entire hole concentration range covered (between 5×10^{19} cm^{-3} and 10^{20} cm^{-3}), and more importantly, larger than those measured for the other samples. A straightforward comparison of the experimental values indicates that the increase in *S* due to the Sn resonance is roughly 50 μV K^{-1}. This enhancement is similar to that observed in In-doped SnTe where an increase between 25 and 65 μV K^{-1} over the values measured on undoped samples have been obtained 5. Although this effect is not as large as that observed in Sn-doped Bi_2Te_3, for which an increase from 100 – 140 μV K^{-1} to 210 – 220 μV K^{-1} (depending on the sample and the reference value considered) has been reported 2, the effect of Sn-induced RL in β-As_2Te_3 is clearly visible. These experimental results are consistent with our DFT calculations and confirm that Sn behaves as a resonant impurity in β-As_2Te_3 while Ga and I act as conventional doping species. The presence of RL in the valence bands of β-As_2Te_3 explains the higher thermopower values measured in the series β-$As_{2-x}Sn_xTe_3$ which, combined with very low lattice thermal conductivity, are at the origin of the good thermoelectric performances achieved at mid temperatures.

4. Conclusion

Our joint theoretical and experimental investigation provides conclusive evidence that Sn forms a resonant level in β-As_2Te_3 that sufficiently distorts the valence band edge to induce an increase in

thermopower. Our calculations of the energy dependence of the density of states show that the sharp resonance peak hybridizes with electronic states of As_2Te_3 for Sn concentrations close to those achieved experimentally. The enhancement of the thermopower in Sn-substituted samples beyond the values predicted by calculations for conventional doping impurities have been experimentally confirmed by the Ioffe-Pisarenko plot of the evolution of the thermopower as a function of the hole concentration. A comparison with the values measured on three series of substituted samples with Ga, Bi and I evidenced the higher values achieved with Sn compared to the other three elements. In addition, further improvement in the thermoelectric performances of β-As_2Te_3 may be possible if its electrical conductivity can be improved by a careful control of its inherent defect chemistry or by using a double-doping strategy. Finally, further detailed calculations would be worthwhile to determine whether Sn, and possibly other elements, can also lead to the formation of resonant states in the sister compound α-As_2Te_3.

Conflicts of interest

There are no conflicts of interest to declare.

Acknowledgements

B.W. and J.T. were supported by the Polish National Science Center (project No. DEC 2011/02/A/ST3/00124) and partially by the AGH UST statutory tasks No. 11.11.220.01/5 within subsidy of the Ministry of Science and Higher Education. J.-B.V., C. C. and B. L. acknowledge the financial support from the French National Research Agency (ANR) in the frame of its program "PROGELEC" (Verre Thermo-Générateur "VTG").

Figures

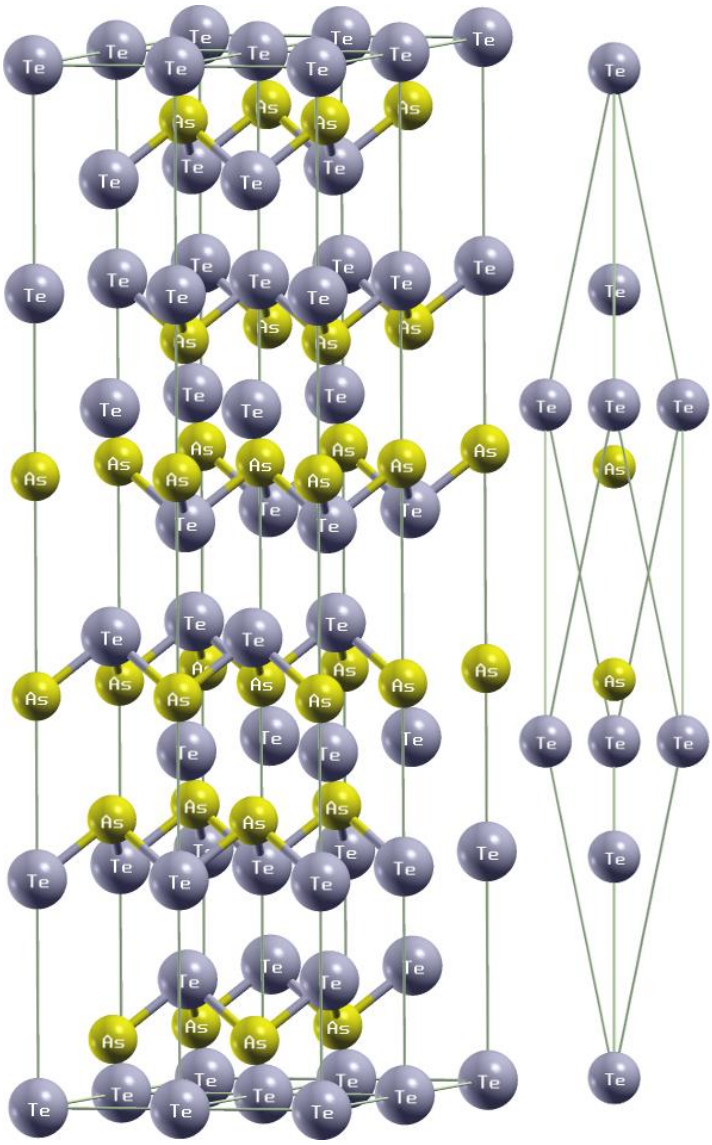

Fig. 1. Tetradymite crystal structure of β-As_2Te_3: hexagonal unit cell (left) and rhombohedral primitive cell (right).

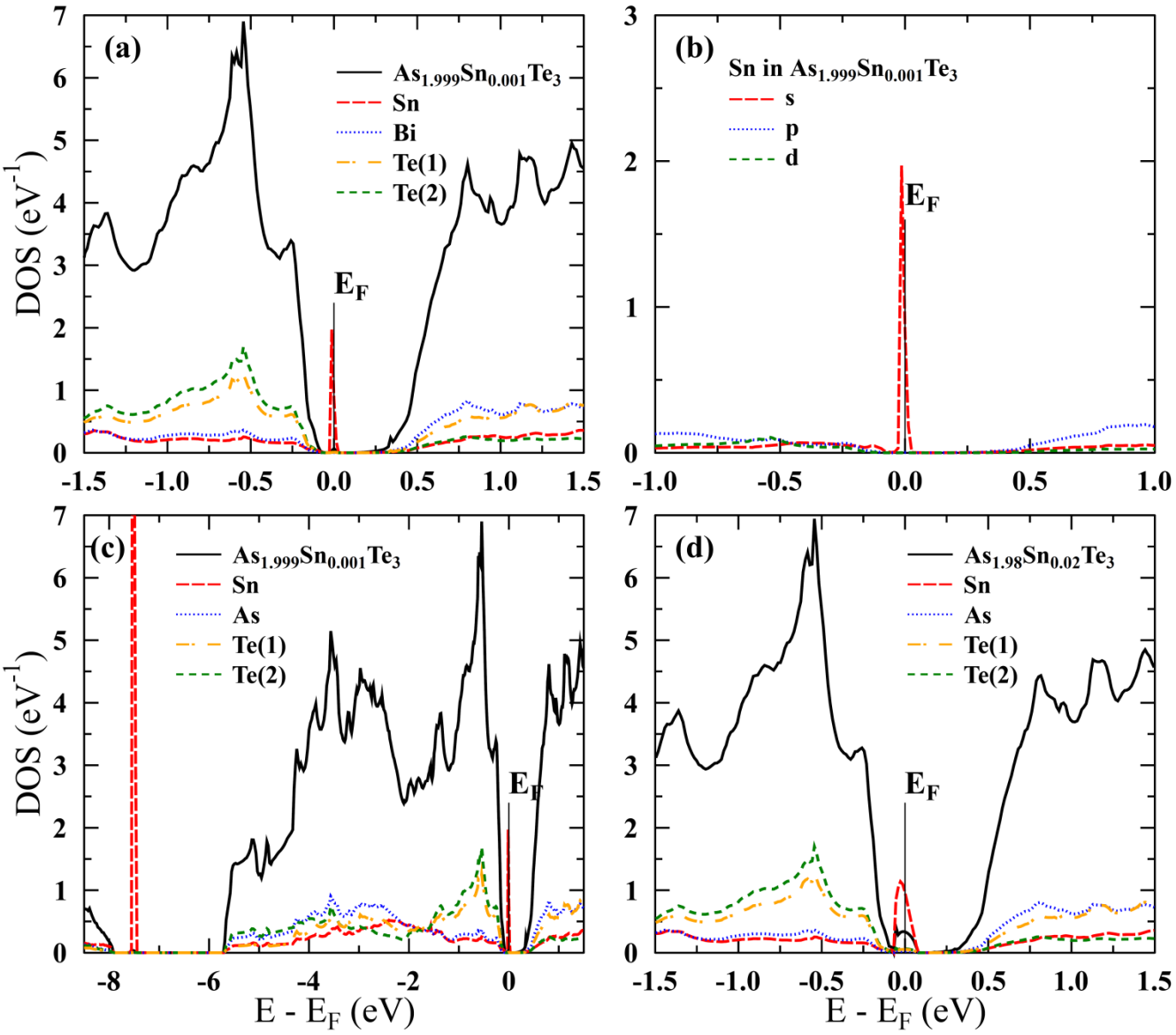

Fig. 2. Energy dependence of the electronic density of states (DOS) for Sn-substituted β-As_2Te_3 for (a-c) 0.1% of Sn and (d) 2% of Sn, as calculated by the KKR-CPA method. Color lines show the atomic contributions per single atom (not weighted by their concentration). Panel (a) shows the position of the Sn-resonance peak at the valence band edge. Panel (b) shows the angular-momentum decomposition of the resonance peak demonstrating that it originates from the 5*s* orbitals of Sn. Panel (c) shows the DOS in broader energy range, where the second, hyper-deep resonant peak is formed near -7.5 eV. Panel (d) shows the DOS for 2% Sn concentration, where the broadening and hybridization of the RL states with the host states are observed.

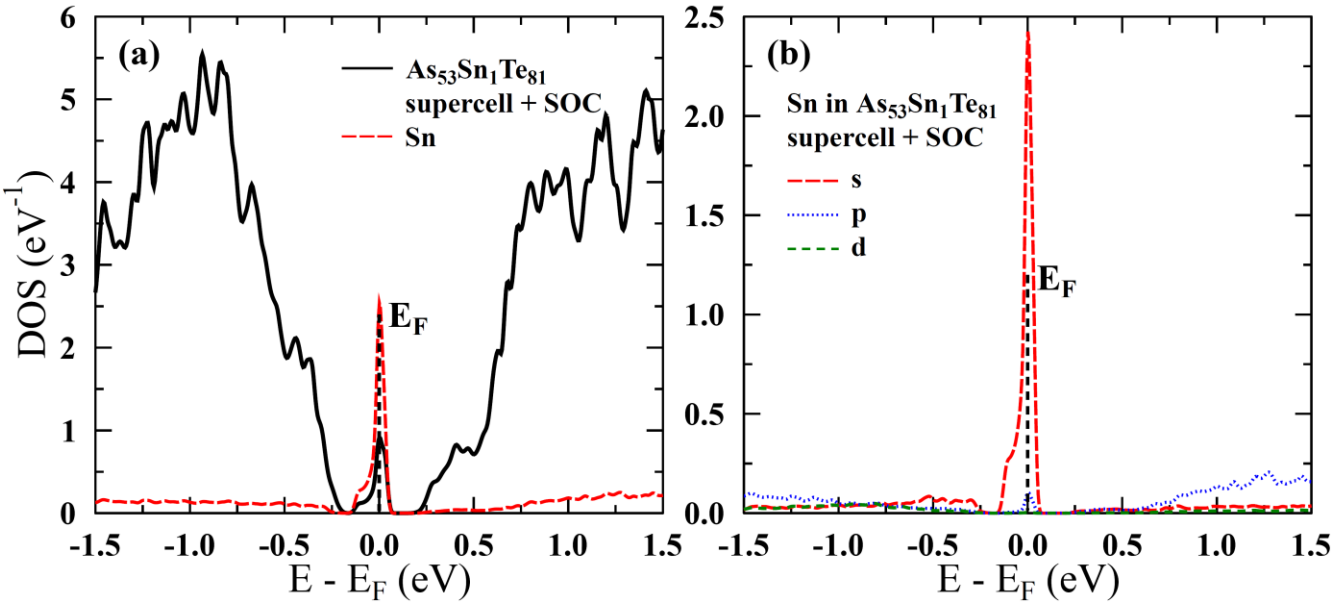

Fig. 3. DOS of the supercell model $As_{53}Sn_1Te_{81}$ (i.e. $As_{1.963}Sn_{0.037}Te_3$), where atomic positions were relaxed after introducing Sn atom into the crystal structure, as computed by the FP-LAPW method. (a) Total DOS (recalculated per As_2Te_3 formula unit) and Sn partial DOS (per atom) as a function of the energy. (b) Partial Sn DOS with angular momentum decomposition. These calculations include the effect of spin-orbit coupling. The resonant state is neither influenced by the local lattice relaxation nor by the spin-orbit coupling.

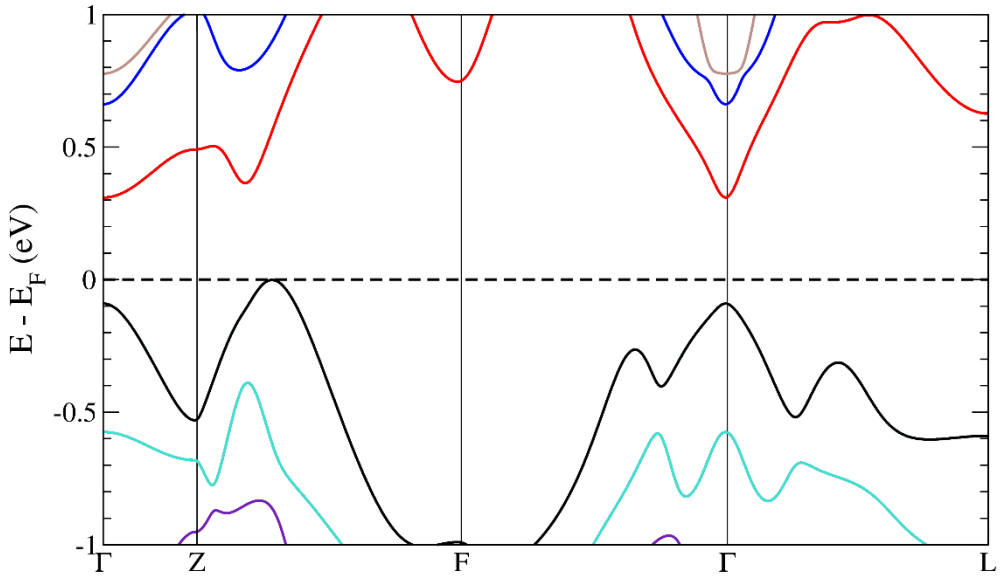

Fig. 4. Magnification of the electronic band structure of β-As_2Te_3 near the Fermi level. Indirect band gap equal to E_g = 0.3 eV is obtained, with the valence band maximum located on the "mirror plane" at a *k*-point close to the Z-F line (see the Fermi surface plot in Figure 5).

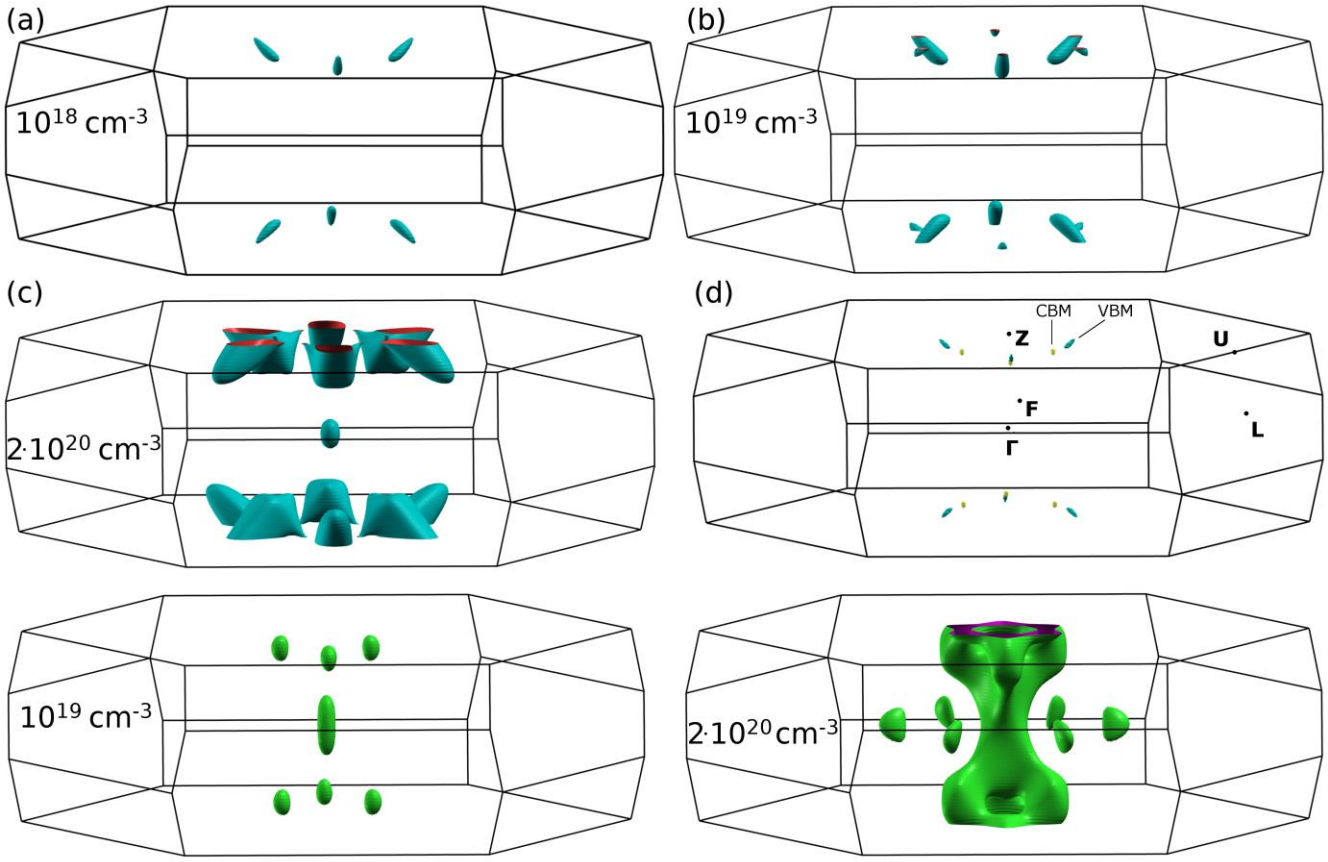

Fig. 5. Fermi surface (FS) of *p*- and *n*-type β-As_2Te_3 computed for carrier concentrations: (a) $p = 10^{18}$ cm^{-3}, (b) $p = 10^{19}$ cm^{-3}, (c) $p = 2 \times 10^{20}$ cm^{-3}, (e) $n = 10^{19}$ cm^{-3}, (f) $n = 2 \times 10^{20}$ cm^{-3}. In panel (d), the isoenergetical surfaces for the conduction (valence) band at 2 meV above (below) band edges are plotted to better visualize the indirect structure of the band gap.

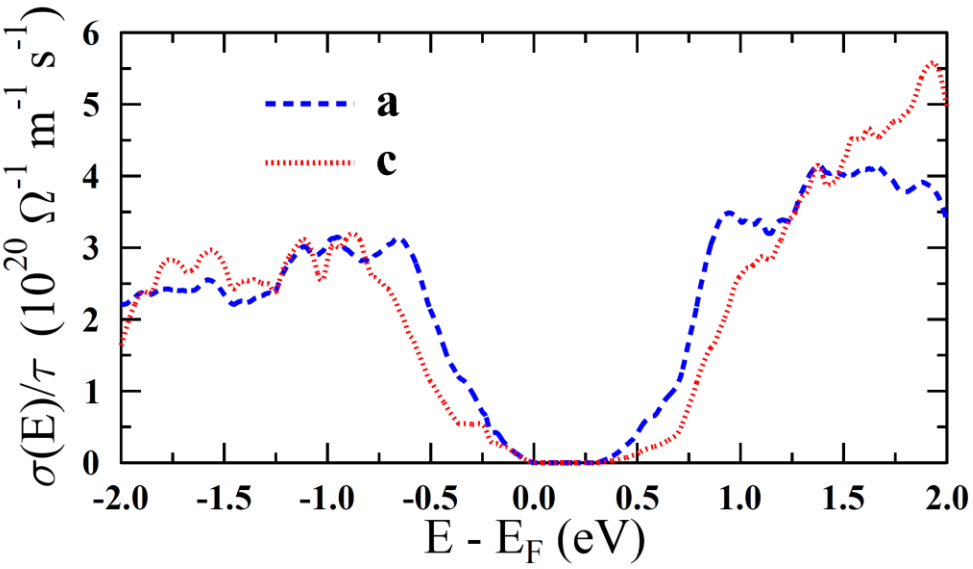

Fig. 6. Energy-dependent electrical conductivity (*i.e.* transport function TF) divided by the scattering time, $\sigma(E)/\tau$, along the binary (a) and trigonal (c) axes.

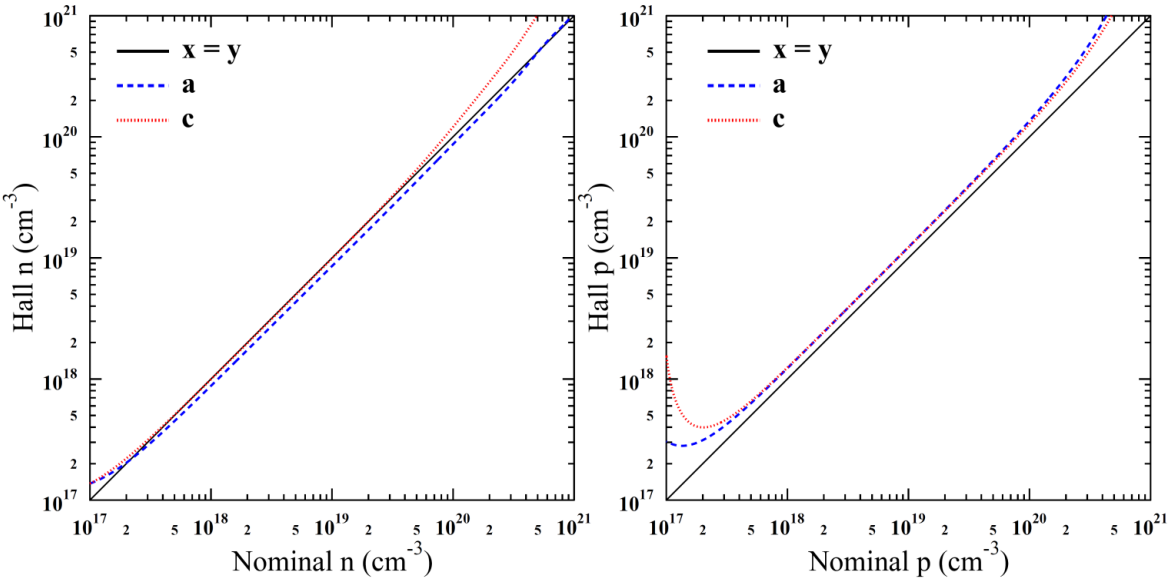

Fig. 7. Computed Hall carrier concentration versus nominal carrier concentration in *n*- and *p*-type β-As_2Te_3, along the *a* and *c* axes. In the 10^{18} cm^{-3} – 10^{20} cm^{-3} concentration range, deviations from the $x = y$ line, as well as anisotropy, are very small.

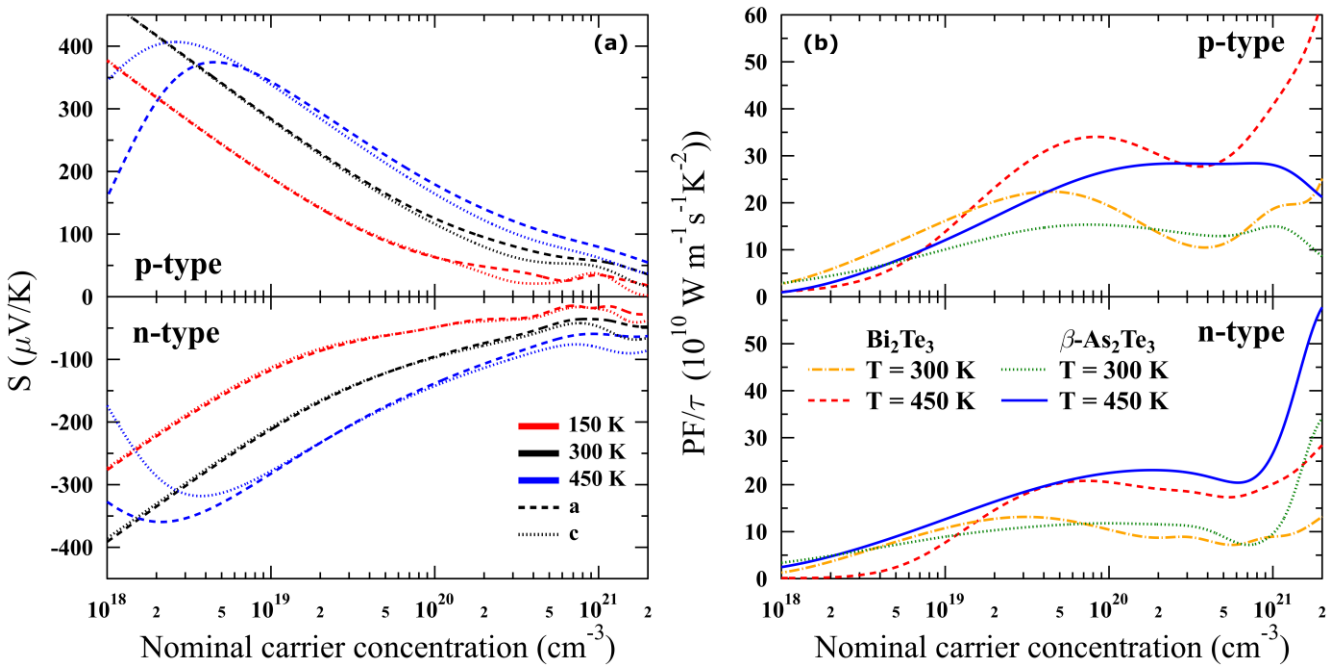

Fig. 8. (a) Thermopower of *p*- and *n*-type β-As_2Te_3 along the binary (*a*) and trigonal (*c*) axis calculated at three selected temperatures. In agreement with experimental results, the anisotropy is very small. (b) Average power factor (PF) divided by the scattering time τ for β-As_2Te_3. For comparison purposes, the results are compared to those obtained for Bi_2Te_3.

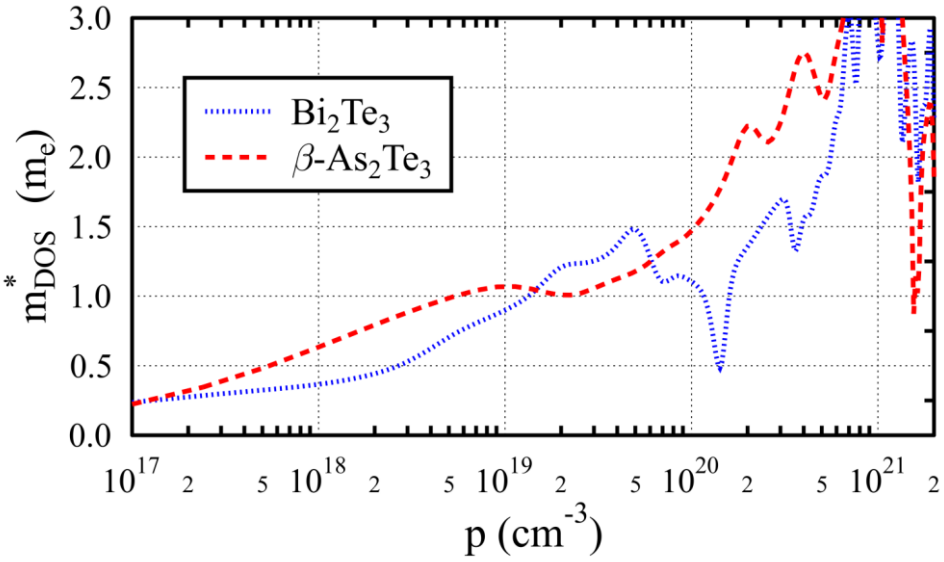

Fig. 9. Computed density-of-states effective mass m^*_{DOS} as a function of the hole concentration *p* for β-As_2Te_3, compared to Bi_2Te_3. Between $p = 10^{19}$ and 10^{20} cm^{-3}, m^*_{DOS} varies in the range 1.0 – 1.5 m_e, in agreement with the value m^*_{DOS} = 1.14 m_e inferred from the SPB model.

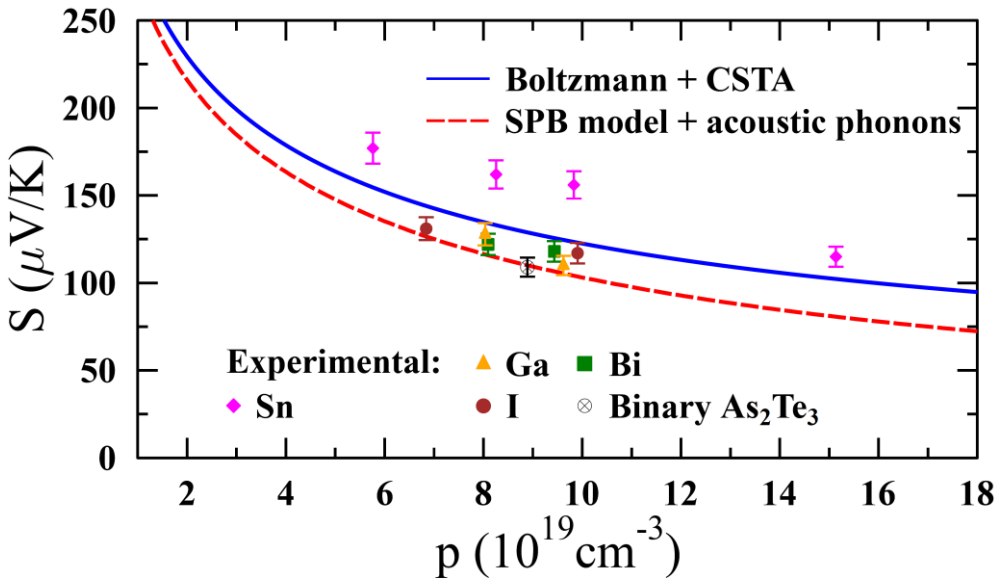

Fig. 10. Ioffe-Pisarenko plot (thermopower *versus* hole concentration) at T = 300 K. The solid blue curve is computed from first principles for pristine β-As_2Te_3 within the Boltzmann approach and constant scattering time approximation (CSTA). The dashed red line is computed using single parabolic band (SPB) model with constant $m^*_{DOS} = 1.14\, m_e$ and assuming an energy-dependent scattering time $\tau = \tau_0 E^{-\frac{1}{2}}$ (acoustic phonon scattering). The experimental thermopower values measured in the β-$As_{2-y}Ga_yTe_3$ (y = 0.01 and 0.03), β-$As_{2-n}Bi_nTe_3$ (n = 0.015 and 0.025) and β-$As_2Te_{3-z}I_z$ (z = 0.01 and 0.02) series have been added for comparison with the β-$As_{2-x}Sn_xTe_3$ series (x = 0.0 – binary As_2Te_3, 0.015, 0.025, 0.035 and 0.050). The increased thermopower values measured in the Sn series, with respect to other impurities and to the theoretical prediction, are well visible. The errors bars correspond to the experimental uncertainty estimated to be 5%.

Table 1

Relaxed crystal structure parameters of β-As_2Te_3 used in our computations, in rhombohedral setting (rhombodedral lattice constant a_{rh} and the rhombohedral angle α_{rh}), which correspond to the hexagonal values of a = 4.094 Å and c = 30.143 Å. In space group $R\bar{3}m$ (no. 166), *u* is the parameter of the 2*c* (*u, u, u*) site occupied by As atoms and *v* is the parameter of the 2*c* (*v, v, v*) site occupied by Te(1) atoms. The Te(2) atoms occupy the 1*a* site with fixed coordinates (0, 0, 0).

a_{rh} (Å)	α_{rh} (°)	*u*	*v*
10.322	22.877	0.3946	0.2192

Table 2

Atomic concentrations, Hall carrier concentrations and room-temperature thermopower values of $As_{2-x}M_xTe_3$ (*M* = Sn, Bi, Ga) and $As_2Te_{3-x}I_x$, used to construct the Ioffe-Pisarenko plot in Fig. 10.

Dopant	Atomic concentration *x*	Carrier concentration *p* (10^{19} cm^{-3})	Thermopower at T = 300 K *S* (μV/K)
Sn	0.000	8.89	109
	0.015	8.26	162
	0.025	5.76	177
	0.035	9.83	156
	0.050	15.14	115
Bi	0.015	8.09	122
	0.025	9.44	118
Ga	0.010	9.62	110
	0.030	8.03	128
I	0.010	9.91	117
	0.020	6.84	131

References

1 J.P. Heremans, B. Wiendlocha, A.M. Chamoire, Resonant levels in bulk thermoelectric semiconductors" Energy Environ. Sci., 5 (2012), 5510.

2 C.M. Jaworski, V.A. Kulbachinskii, and J.P. Heremans, Tin forms a resonant level in Bi_2Te_3 that enhances the room temperature thermoelectric power. Phys. Rev. B 80 (2009), 233201.

3 J.P. Heremans, V. Jovovic, E.S. Toberer, A. Saramat, K. Kurosaki, A. Charoenphakdee, S. Yamanaka, G.J. Snyder, Enhancement of thermoelectric efficiency in PbTe by distortion of the electronic density of states, Science 321 (2008), 554–558.

4 C.M. Jaworski, B. Wiendlocha, V. Jovovic, J.P. Heremans, Combining alloy scattering of phonons and resonant electronic levels to reach a high thermoelectric figure of merit in PbTeSe and PbTeS alloys, Energy Environ. Sci. 4 (2011), 4155–4162.

5 Q. Zhang, B.L. Liao, Y.C. Lan, K. Lukas, W.S. Liu, K. Esfarjani, C. Opeil, D. Broido, G. Chen, Z.F. Ren, High thermoelectric performance by resonant dopant indium in nanostructured SnTe. Proc. Nat. Acad. Sci. USA 110 (2013), 13261–13266.

6 J.D. König, M.D. Nielsen, Y.B. Gao, M. Winkler, A. Jacquot, H. Böttner, J.P. Heremans, Titanium forms a resonant level in the conduction band of PbTe, Phys. Rev. B 84 (2011), 205126.

7 B. Wiendlocha, Localization and magnetism of the resonant impurity states in Ti doped PbTe, Appl. Phys. Lett. 105 (2014), 133901.

8 B. Wiendlocha, K. Kutorasinski, S. Kaprzyk, J. Tobola, Recent progress in calculations of electronic and transport properties of disordered thermoelectric materials, Scripta Materialia 111 (2016), 33.

9 B. Wiendlocha, Fermi surface and electron dispersion of PbTe doped with resonant Tl impurity from KKR-CPA calculations, Physical Review B 88 (2013), 205205 .

10 J.P. Heremans, B. Wiendlocha, H. Jin, Thermoelectric Materials with Resonant States, in *Advanced Thermoelectrics: Materials, Contacts, Devices, and Systems*, ed. Z. Ren, Y. Lan, Qi. Zhang, CRC Press, Taylor & Francis Group, Boca Raton, FL (USA), 2017.

11 J. P. Heremans and B. Wiendlocha, Tetradymites: Bi_2Te_3-Related Materials, in *Materials Aspect of Thermoelectricity*, ed. Ctirad Uher, CRC Press, Taylor & Francis Group, Boca Raton, FL (USA), 2017.

12 J.-B. Vaney, J. Carreaud, G. Delaizir, A. Pradel, A. Piarristeguy, C. Morin, E. Alleno, J. Monnier, A.P. Gonçalves, C. Candolfi, A. Dauscher, B. Lenoir, High-Temperature Thermoelectric Properties of Sn-Doped β-As_2Te_3, Adv. Electron. Mater.,1: doi: 10.1002/aelm.201400008.

13 J.-B. Vaney , J. Carreaud, G. Delaizir, C. Morin, J. Monnier, E. Alleno, A. Piarristeguy, A. Pradel, A.P. Gonçalves, E.B. Lopes, C. Candolfi, A. Dauscher, B. Lenoir, Thermoelectric Properties of the α-As_2Te_3 Crystalline Phase, J. Electronic Mater. 45 (2016), 1447.

14 J.-B. Vaney, G. Delaizir, B. Wiendlocha, J. Tobola, E. Alleno, A. Piarristeguy, A.P. Gonçalves, C. Gendarme, B. Malaman, A. Dauscher, C. Candolfi, and B. Lenoir, "Effect of Isovalent Substitution on the Electronic Structure and Thermoelectric Properties of the Solid Solution α-$As_2Te_{3-x}Se_x$ ($0 \leq x \leq 1.5$)", Inorganic Chemistry 56 (2017), 2248

15 J.-B. Vaney, J. Carreaud, G. Delaizir, A. Piarristeguy, A. Pradel, E. Alleno, J. Monnier, E. B. Lopes, A. P. Gonçalves, C. Candolfi, A. Dauscher, B. Lenoir, "High Thermoelectric Performance in Sn-Substituted α-As_2Te_3" Journal of Materials Chemistry C, 4 (2016), 2329

16 C. Morin, S. Corallini, J. Carreaud, J.-B. Vaney, G. Delaizir, J. C. Crivello, E. B. Lopes, A. Piarristeguy, J. Monnier, C. Candolfi, V. Nassif, G. Cuello, M. Ribes, A. Pradel, A. P. Gonçalves, B. Lenoir, E. Alleno, "Polymorphism in

thermoelectric As_2Te_3", Inorganic Chemistry, 54 (2015), 9936

17 J.-B. Vaney, G. Delaizir, A. Piarristeguy, J. Monnier, E. Alleno, E. B. Lopes A. P. Gonçalves, A. Pradel, A. Dauscher, C. Candolfi, B. Lenoir , "High-temperature thermoelectric properties of the β-$As_{2-x}Bi_xTe_3$ solid solution", APL Materials, 4 (2016), 104901

18 J.-B. Vaney, J.-C. Crivello, C. Morin, G. Delaizir, J. Carreaud, A. Piarristeguy, J. Monnier, E. Alleno, A. Pradel, E. B. Lopes A. P. Gonçalves, A. Dauscher, C. Candolfi, B. Lenoir , "Electronic structure, low-temperature transport and thermodynamic properties of polymorphic β-As_2Te_3", RSC Advances, 6 (2016), 52048.

19 A. Bansil, S. Kaprzyk, P.E. Mijnarends, J. Tobola, Electronic structure and magnetism of $Fe_{3-x}V_xX$ (X = Si, Ga, and Al) alloys by the KKR-CPA method, Phys. Rev. B 60 (1999), 13396 – 13412.

20 T. Stopa, S. Kaprzyk, J. Tobola, Linear aspects of the Korringa–Kohn–Rostoker formalism, J. Phys.: Condens. Matter 16 (2004), 4921 – 4933.

21 J.P. Perdew, Y. Wang, Accurate and simple analytic representation of the electron-gas correlation energy, Phys. Rev. B 45 (1992), 13244 – 13249.

22 S. Kaprzyk, A. Bansil, Green's function and a generalized Lloyd formula for the density of states in disordered muffin-tin alloys, Phys. Rev. B 42 (1990), 7358 – 7362.

23 P. Blaha, K. Schwarz, G. K. H. Madsen, D. Kvasnicka, and J. Luitz, WIEN2K, An Augmented Plane Wave Local Orbitals Program for Calculating Crystal Properties, Karlheinz Schwarz, Techn. Universitat Wien, Austria, 2001.

24 F. Tran, P. Blaha, Accurate Band Gaps of Semiconductors and Insulators with a Semilocal Exchange-Correlation Potential, Phys. Rev. Lett. 102 (2009), 226401.

25 G.K.H. Madsen, D.J. Singh, BoltzTraP. A code for calculating band-structure dependent quantities, Comput. Phys. Commun. 175 (2006), 67.

26 J.-B. Vaney , J. Carreaud, G. Delaizir, C. Morin, J. Monnier, E. Alleno, A. Piarristeguy, A. Pradel, A.P. Gonçalves, E.B. Lopes, C. Candolfi, A. Dauscher, B. Lenoir, Low-Temperature Transport Properties of Bi-substituted β-As_2Te_3, Journal of Electronic Materials 45 (2016), 1786.

27 Sharma, Y.; Srivastava, P. First principles investigation of electronic, optical and transport properties of α- and β-phase of arsenic telluride. Opt. Mater.33 (2011), 899 – 904.

28 B. Wiendlocha, Resonant Levels, Vacancies, and Doping in Bi_2Te_3, Bi_2Te_2Se, and Bi_2Se_3 Tetradymites, Journal of Electronic Materials 45 (2016), 3515.

29 H. Jin, B. Wiendlocha, J.P. Heremans, P-type doping of elemental bismuth with indium, gallium and tin: a novel doping mechanism in solids, Energy Environ. Sci. 8 (2015), 2027.

30 T.J. Scheidemantel, J.V. Badding, Electronic structure of β-As_2Te_3, Solid State Communications 127 (2003), 667.

31 K. Kutorasinski, B. Wiendlocha, J. Tobola, and S. Kaprzyk, "Importance of relativistic effects in electronic structure and thermopower calculations for Mg_2Si, Mg_2Ge, and Mg_2Sn", Phys. Rev. B 89 (2014), 115205.

32 K. Kutorasinski, B. Wiendlocha, S. Kaprzyk, and J. Tobola, "Electronic structure and thermoelectric properties of n- and p-type SnSe from first-principles calculations", Physical Review B 91 (2015), 205201.

33 B. Wiendlocha, presented at the 15th European Conference on Thermoelectrics (ECT2017), Padova, Italy, 25-27.09.2017, to be published.